

DOI: 10.1002/ajoc.201700563

Full Paper

**Multiple Photoluminescence from Pyrene-Fused Hexaarylbenzenes with Aggregation-Enhanced Emission Features**

Chuan-Zeng Wang,<sup>[a]</sup> Yuki Noda,<sup>[a]</sup> Chong Wu,<sup>[a]</sup> Dr. Xing Feng,<sup>\*[b]</sup>  
Dr. Perumal Venkatesan,<sup>[c]</sup> Prof. Hang Cong,<sup>[d]</sup> Dr. Mark<sup>^^</sup>R.<sup>^^</sup>J.  
Elsegood,<sup>[e]</sup> Thomas<sup>^^</sup>G. Warwick,<sup>[e]</sup> Dr. Simon<sup>^^</sup>J. Teat,<sup>[f]</sup> Prof.  
Carl Redshaw,<sup>[g]</sup> and Prof. Takehiko Yamato 0000-0002-8812-  
2242<sup>\*[a]</sup>

[a] <orgDiv/>Department of Applied Chemistry  
<orgDiv/>Faculty of Science and Engineering  
<orgName/>Saga University  
<street/>Honjo-machi 1  
<city/>Saga <postCode/>840-8502 (<country/>Japan)  
E-mail: yamatot@cc.saga-u.ac.jp

[b] <orgDiv/>Faculty of Material and Energy Engineering  
<orgName/>Guangdong University of Technology  
<city/>Guangzhou <postCode/>510006 (<country/>P.<sup>^^</sup>R.  
China)  
E-mail: hyxhn@sina.com

[c] <orgDiv/>Lab. de Polímeros  
Centro de Química, Instituto de Ciencias  
<orgName/>Benemérita Universidad Autónoma de Puebla  
Complejo de Ciencias, ICUAP, Edif. 103H  
<street/>22 Sur y San Claudio  
<city/>Puebla, Puebla C.P. <postCode/>72570  
(<country/>Mexico)

- [d] <orgName/>Guizhou University  
<city/>Guiyang <postCode/>550025 (<country/>P.^R. China)
- [e] <orgDiv/>Chemistry Department  
<orgName/>Loughborough University  
<city/>Loughborough, <postCode/>LE11 3TU (<country/>UK)
- [f] <orgName/>ALS Berkeley Lab  
<street/>1 Cyclotron Road  
<city/>Berkeley, <countryPart/>CA <postCode/>94720  
(<country/>USA)
- [g] <orgDiv/>Department of Chemistry  
<orgName/>The University of Hull  
<street/>Cottingham Road  
<city/>Hull, <postCode/>HU6 7RX (<country/>UK)

<pictid> Supporting information and the ORCID identification number(s) for the author(s) of this article can be found under <url><https://doi.org/10.1002/ajoc.201700563></url>.

**Checking into reHAB:** Multiple photoluminescence, which included monomer emission, excimer emission, and charge-transfer emission processes, has been observed from new pyrene-fused hexaarylbenzenes (HABs). X-ray diffraction analysis clearly indicated that the pyrene moieties adopted different crystal packing arrangements in the crystalline state that could induce a multiple-photoluminescence phenomenon.

Multiple #photoluminescence has been observed from new pyrene-fused #hexaarylbenzenes (HABs) @BUAPoficial @lborouniversity @BerkeleyLab @UniOfHull

aggregation  
hexaarylbenzenes  
luminescence  
photochemistry  
pyrenes

Multiple photoluminescence, which included monomer emission, excimer emission, and charge-transfer emission processes, has been observed from new pyrene-fused hexaarylbenzene (HAB) compounds, which were synthesized in high yields through a Diels--Alder reaction between bis(2-*tert*-butylpyren-6-yl)acetylene and tetraphenylcyclopentadienone. Although the differentiation between two molecules only arose from the geometrical position of one of the pyrenes, the NMR spectra, crystal packing, and physicochemical properties of these pyrene-based HAB hybrids were distinctly different in both the solution and aggregate states. X-ray diffraction analysis clearly indicated that the pyrene moieties adopted different crystal packing arrangements in the crystalline state that could induce a multiple-photoluminescence phenomenon.

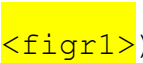
## Introduction

The construction of intriguing molecular structures is both an art and a science, and has attracted considerable interest in recent years. Highlights include carborane-cage-based dyads with aryl substitution,<sup>[1]</sup> propeller-shaped tetraphenylethene-based aggregation-induced emission (AIE) luminogens with bulky pendant groups,<sup>[2]</sup> chiral helicenes with fused planar and nonplanar systems,<sup>[3]</sup> and  $\pi$ -expanded fullerene-based dyads.<sup>[4]</sup> Such systems have played a crucial role in the development of organic optoelectronics. Among the

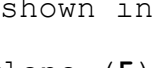
many promising candidate structures, hexaarylbenzene (HAB) appears to be an ideal scaffold, because it possesses a rigid core and adjustable aryl units, which allow for the formation of unusual and fascinating structures. It has also been possible to extend the range of possible applications for HAB derivatives by the introduction of suitable radial-substitution reactions.<sup>[5]</sup>

Pyrenes, as typical polycyclic aromatic hydrocarbons (PAHs), possess unique optoelectronic properties, in particular favorable stability and high fluorescence efficiency, as well as features that can be readily modified, which have led to their extensive exploration as fluorophores.<sup>[6]</sup> Efficient monomeric emission within the range  $\lambda=370\text{--}430\text{ nm}$  and excimer emission at  $\lambda>480\text{ nm}$ ,<sup>[7]</sup> combined with possible charge-transfer (CT) emission through the introduction of appropriate donor/acceptor moieties, have established their position/reputation in comparison with other polyaromatic fluorophores (Scheme<sup>1</sup>).<sup>[8]</sup> However, the mechanisms that are associated with multiple photoluminescence from a single molecule in pyrene chemistry remains relatively unexplored. The minimal mechanistic work to date reflects the limiting harsh prerequisites, such as the combination of multidimensional intermolecular interactions, predetermined spatial arrangements, and appropriate donor/acceptor groups.<sup>[9]</sup> Thus, the design and synthesis of organic molecules with multiple photoluminescence remains a challenge.

Building on the individual emission mechanisms mentioned above, we conceived a new strategy for the construction of high-performance single molecules that exhibit multiple

photoluminescence. Our aim was to integrate a pyrene fluorophore with a propeller-shaped HAB scaffold into a single molecule that would exhibit multiple photoluminescence, owing to its multidimensional geometrical parameters, conformations, and intra/intermolecular interactions. We wanted to construct this "propeller" by replacing two of the "propeller blades". Herein, we report the synthesis of two pyrene-based HAB derivatives, *anti*-**6** and *syn*-**6**. Gratifyingly, we obtained single crystals of these two conformers by the slow diffusion of MeOH vapor into a solution of each conformer in CHCl<sub>3</sub>, which allowed us to determine the intriguing structures of *anti*-**6** and *syn*-**6** by using X-ray crystallography (Figure<sup>^1</sup>).

## Results and Discussion

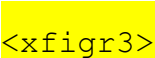
As shown in Scheme<sup>^2</sup>, bis(2-*tert*-butylpyren-6-yl)acetylene (**5**) was synthesized through a Sonogashira coupling reaction between 1-bromo-7-*tert*-butylpyrene (**2**) and 7-*tert*-butyl-1-ethynylpyrene (**4**) in 75% yield. Next, 1,2-bis(7-*tert*-butylpyren-1-yl)-3,4,5,6-(tetraphenyl)benzenes (*anti*-**6** and *syn*-**6**) were prepared from the Diels--Alder reaction of bis(2-*tert*-butylpyren-6-yl)acetylene (**5**) with 2,3,4,5-tetraphenylcyclopenta-2,4-dienone in one step (for full synthetic procedures and characterization data, see the Supporting Information). These two stereoisomers were cleanly separated by standard column chromatography on silica gel and recrystallization, thereby affording *anti*-**6** as a pale-green solid and *syn*-**6** as a yellow solid in 53% and 22% yield, respectively. <sup>1</sup>H and <sup>13</sup>C<sup>^</sup>NMR spectroscopy, X-ray crystallography, and HRMS clearly indicated that these products were different compounds. Both compounds exhibited

excellent thermal stability, with decomposition temperatures ( $T_d$ ) of 411 $^{\circ}\text{C}$  for *anti*-**6** and 403 $^{\circ}\text{C}$  for *syn*-**6** under a nitrogen atmosphere at a heating rate of 10 $^{\circ}\text{C}^{\text{min}^{-1}}$ , as shown in Table<sup>^1</sup>[<tabr1>](#) and the Supporting Information, Figure<sup>^S11</sup>. Moreover, the fundamental photophysical properties and reaction mechanism were also investigated, which demonstrated the validity of this strategy for the construction of multiple-photoluminescent molecules.<?><?>sentence ok<?><?>

Analysis of the  $^1\text{H}$ -NMR spectra revealed well-resolved proton signals that allowed us to easily distinguish between these two isomers (Figure<sup>^2</sup>[<figr2>](#)). As expected, for *anti*-**6**, six doublets (12 $^{\text{H}}$ ; owing to *ortho* coupling) and two singlets (4 $^{\text{H}}$ ) were observed for the pyrene moieties, although there was an overlap between one singlet (c';  $\delta$ =8.02 $^{\text{ppm}}$ ; Figure<sup>^2</sup>[<xfigr2>](#)) and one doublet (d';  $\delta$ =8.01 $^{\text{ppm}}$ ; Figure<sup>^2</sup>[<xfigr2>](#)). In comparison, the proton signals for *syn*-**6** exhibited a narrow distribution, especially for the hydrogen atoms in the K-region of the pyrene moieties (d, e--g; 8 $^{\text{H}}$ ;  $\delta$ =7.58--7.70 $^{\text{ppm}}$ ; Figure<sup>^2</sup>[<xfigr2>](#)). In addition, the protons at the 6,8-positions of the pyrene completely coalesced into one singlet (b; 4 $^{\text{H}}$ ;  $\delta$ =7.89 $^{\text{ppm}}$ ; Figure<sup>^2</sup>[<xfigr2>](#)), which reflected the shielding effects that were induced by the spatial overlap of the aromatic rings. In addition, the thermostability and photochemical stability were further studied by using  $^1\text{H}$ -NMR spectroscopy (see the Supporting Information, Figure<sup>^S12</sup>); interconversion between *anti*-**6** and *syn*-**6** was not observed after heating (30 $^{\text{min}}$  at 180 $^{\circ}\text{C}$ ) or irradiation under UV light in air. The NMR spectrum indicated that *anti*-**6** and *syn*-**6** exhibited remarkable conformational stability with unique optical properties.

UV/Vis and photoluminescence (PL) spectra of *anti*-**6** and *syn*-**6** were recorded in dilute THF solution. Both compounds exhibited multiple bands with different shapes in solution, which differed markedly from those of conventional pyrene-based chromophores (Figure<sup>3</sup>[<figr3>](#), left). *Anti*-**6** exhibited three weak, structureless absorptions for the <sup>1</sup>L<sub>b</sub> bands at  $\lambda=403$  nm ( $\log \epsilon_{\max}=2.87$  M<sup>-1</sup> cm<sup>-1</sup>),  $\lambda=353$  nm ( $\log \epsilon_{\max}=4.72$  M<sup>-1</sup> cm<sup>-1</sup>), and  $\lambda=283$  nm ( $\log \epsilon_{\max}=4.67$  M<sup>-1</sup> cm<sup>-1</sup>), which correspond to the S<sub>0</sub>→S<sub>1</sub>, S<sub>0</sub>→S<sub>2</sub>, and S<sub>0</sub>→S<sub>3</sub> transitions, respectively, and were associated with the vibrational fine structure. Owing to the experimental conditions, the S<sub>0</sub>→S<sub>4</sub> transition band in the near-ultraviolet region could not be clearly assigned, which may have originated from the nature of the pyrene structure.<sup>[11]</sup> *Syn*-**6** presented similar absorption properties. The details of the photophysical properties of the two stereoisomers are summarized in Table<sup>1</sup>[<xtabr1>](#).

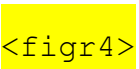
In contrast to their similar absorption spectra, stereoisomers *anti*-**6** and *syn*-**6** exhibited distinct emission bands in solution and in the solid state, owing to their different molecular conformations. Specifically, *anti*-**6** emitted blue light with two well-resolved emission bands at  $\lambda=394$  nm and  $\lambda=447$  nm in THF solution. The shoulder peak at  $\lambda=394$  nm was assigned to the monomeric emission of the pyrene-like chromophore,<sup>[7]</sup> whilst the maximum at  $\lambda=447$  nm was attributed to intermolecular interactions in this propeller-shaped multiple-conjugated system. Similarly, *syn*-**6** also exhibited a blue emission band centered at  $\lambda=412$  nm in THF solution (Figure<sup>3</sup>[<xfigr3>](#) right). Interestingly, new minor peaks for both stereoisomers appeared in the solid state,

which may indicate the presence of different molecular conformations, thus leading to different emission behavior compared with the solution state. As shown in Figure<sup>3</sup> , *anti-6* displayed a red-shifted emission maximum at  $\lambda=482$  nm, with a shoulder peak at  $\lambda=463$  nm, but no clear emission at  $\lambda=394$  nm. It is reasonable to speculate that the new peak at  $\lambda=482$  nm arose from excimer emission, whilst the shoulder peak at  $\lambda=463$  nm may have originated from a significant intermolecular interaction. We speculated that there was an intermolecular charge transfer (InterCT)<sup>[12]</sup> state, thereby resulting in a slight red-shift from the primary peak at  $\lambda=447$  nm in solution to the minor peak at  $\lambda=463$  nm in the solid state. Similar optical characteristics were also observed for *syn-6*. In this system, we could readily assign the monomeric emission and excimer emission in the solution and solid states from the multiple photoluminescence spectra. Taking *anti-6* as an example, we assumed that the emission band at  $\lambda=447$  nm in solution and  $\lambda=463$  nm in the solid state could be attributed to the InterCT emission. Given that the polarity of the solution could exert slight effects on the CT emission, a solvatochromism experiment was performed. As shown in the Supporting Information, Figure<sup>S13</sup>, *anti-6* exhibited a slight red-shift from the less-polar cyclohexane ( $\lambda=442$  nm) to the more-polar DMF ( $\lambda=453$  nm), whilst there was no clear relationship with increasing polarity for the low-wavelength emission band at  $\lambda<394$  nm. This result further demonstrated that there was no intramolecular charge transfer (ICT) for the *anti-6* system, with InterCT observed instead. Unsurprisingly, there was barely a change in the solvatochromism for *syn-6*, consistent with our conjecture and



with the emission properties in solution and in the solid state. Thus, the spectroscopic data strongly supported the presence of multiple photoluminescence from the monomeric emission, excimer emission, and CT emission in this system.

More-detailed information on multiple photoluminescence and its dependence on the molecular conformation could be gleaned from the single-crystal X-ray diffraction analysis of both stereoisomers.

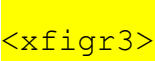
It is well-known that the propeller-shaped HAB scaffold is particularly attractive, owing to its rigid hub and adjustable peripheral groups. The peripheral groups on the HAB scaffold typically undergo interlocking to exhibit interesting structural variations with fascinating photophysical properties. Therefore, we further attempted to interpret the mechanism on the basis of our X-ray crystallographic results. Close inspection revealed that HAB derivatives *anti*-**6** and *syn*-**6** exhibited distinctively different spatial arrangements to each other. As shown in Figure<sup>4</sup> , a shell-like intermolecular donor-acceptor system was observed for *anti*-**6**, which was achieved by utilizing the electron-rich pyrene molecules as the donor "shell", and the electron-deficient phenyl moieties as the acceptor "pearl". The fragments that comprised pyrene-phenyl-pyrene moieties displaced face-to-face patterns that were linked through C-H...M...M...M-π interactions, with distances of 2.79--2.87 Å. The pyrene moieties were almost mutually perpendicular. The formation of a donor-acceptor system was preferred to the formation of a charge-transfer system. More interestingly, clear InterCT was observed, as demonstrated by experimental and crystallographic

studies, with a maximum InterCT emission at  $\lambda=447$  nm in THF solution. In contrast to *anti*-**6**, a clear pyrene $\pi$ -pyrene  $\pi$  stacking interaction with a distance of 3.15 Å was observed in the packing of *syn*-**6**. Clearly, the  $\pi$  stacking interaction played a dominant role in the emission. The most-direct evidence was that the excimer emission peak at  $\lambda=484$  nm appeared in the solid state, but was not observed in solution. These results provided powerful evidence for the emission phenomenon and mechanism.

In general, HAB homologues exhibit pronounced AIE properties. To further investigate their AIE properties, the PL spectra of *anti*-**6** and *syn*-**6** ( $5 \times 10^{-7}$  M) were recorded in water/THF mixtures with different water content (Figure 5a). Taking *anti*-**6** as an example, interesting aggregation-enhanced emission (AEE) behavior was observed.<sup>[13]</sup> In particular, on increasing the water fraction in the water/THF mixture from 0% to 60%, the emission intensity was enhanced about two-fold (solid line; Figure 5a), owing to restricted intramolecular rotation (RIR), which led to enhanced emission in this propeller-shaped system.<sup>[13c]</sup> However, when the water content was increased to 99%, the emission gradually decreased and a new peak was observed in THF solution (dashed line; Figure 5a), which resulted from the formation of excimer emission and solvent-polarity-dependent InterCT emission.<sup>[14]</sup> Notably, the emission profiles presented a coherent transition from pure organic solution to solvent mixtures, aggregates, and the solid state. In the pure organic phase, two well-separated emission bands were observed as

monomeric emission ( $\lambda=394$  nm) and CT emission ( $\lambda=447$  nm), and this type of emission band remained unaltered until the water percentage was increased to 60%, which induced the formation of aggregates. Gradually, as the water fraction increased above 60%, multiple emission spectra gradually appeared, owing to monomeric emission ( $\lambda=416$  nm), CT emission ( $\lambda=453$  nm), and excimer formation ( $\lambda=481$  nm). In the solid state, the PL spectra suggested that excimer emission played a dominant role, whilst the CT emission was secondary. Similar AEE properties and transitions for the emission could also be observed for *syn-6* (see the Supporting Information, Figure<sup>S14</sup>). In the case of *syn-6*, there were two main emissions: monomeric emission ( $\lambda=412$  nm) and excimer emission ( $\lambda=484$  nm). Notably, concentration-dependent luminescence was observed for these two compounds, in excellent agreement with their AEE properties (see the Supporting Information, Figures<sup>S15</sup> and <sup>S16</sup>). Increasing emission intensity was observed on increasing the concentration until the luminescence reached maximum intensity, following which the luminescence decreased when the concentration was further increased; similar red-shifts and multiple photoluminescence were also observed. Furthermore, the fluorescence quantum yields were recorded in solution and in the solid state, and the quantum yields ( $\Phi_{\text{PL}}$ ) are listed in Table<sup>1</sup> [<xtabr1>](#). Specifically, notable enhancement in the quantum yield from 60% (in THF solution) to 95% (at 60% water fraction) was observed for *anti-6*, whilst a subdued quantum yield (45%) was observed in the solid state, owing to excimer formation. Similar optical behavior was observed for *syn-6*.

To provide further evidence for the energy states, cyclic voltammetry (CV) and DFT calculations (B3LYP/6-31G\*) were performed for *anti*-**6** and *syn*-**6** to interpret the electronic states in combination with their photophysical properties. As shown in the Supporting Information, Figure<sup>^</sup>S18, both compounds displayed irreversible redox processes with distinct positive potentials at about 1.4<sup>^</sup>V in solution. As shown in the Supporting Information, Figures<sup>^</sup>S19 and S20, the electronic distributions of compounds **6** in the ground state were further studied by using frontier orbital analysis. As expected, both optimized geometries were consistent with their single-crystal X-ray structures (see the Supporting Information, Table<sup>^</sup>S1). Next, time-dependent DFT (TD-DFT) calculations were performed by using the Gaussian program package at the B3LYP/6-31G\* level of theory. Simulated electronic spectra were also produced based on the TD-DFT results, which were largely consistent with the experimental results. The TD-DFT calculations showed that the pyrene moiety played a dominant role in the orbital transition for the electronic excitation, according to the respective contributions. In this system, the stronger  $S_0 \rightarrow S_4$  transition was described by almost 50:50 contributions of the  $\text{HOMO}_{\text{M}} \rightarrow \text{LUMO}_{\text{M+1}}$  and  $\text{HOMO}_{\text{M-1}} \rightarrow \text{LUMO}_{\text{M}}$  transitions to the shoulder absorption band of *anti*-**6**; thus, these three key frontier molecular orbitals should be considered in any discussion of this system. Specifically, the shoulder absorption was owing to different combinations of the  $\text{HOMO}_{\text{M}} \rightarrow \text{LUMO}_{\text{M+1}}$  and  $\text{HOMO}_{\text{M-1}} \rightarrow \text{LUMO}_{\text{M}}$  transitions with a very high oscillator strength ( $f=0.416$ , and  $f=0.289$ ), and a low oscillator strength of 0.078 for  $S_0 \rightarrow S_n$  ( $n=1-3$ ). These

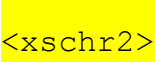
theoretical results provided further insight into the intensity of the absorption spectra, as shown in Figure<sup>3</sup>. The detailed results of the TD-DFT calculations for the ground-state-optimized geometries for *anti*-**6** and *syn*-**6** are presented in the Supporting Information, along with the simulated absorption spectra.

## Conclusion

In summary, by using a propeller-shaped HAB scaffold, we have observed intriguing multiple photoluminescence. Thermally stable *anti*-**6** and *syn*-**6** pyrene-fused hexaarylbenzenes exhibited unusual AEE characteristics. Multiple emission mechanisms, including monomer, excimer, and CT emission processes, were identified in a single molecule. Single-crystal X-ray structures of these two compounds provided further insight into their differing properties. We envision that this work will widen our thinking in photophysics and stimulate work on innovative light-based technologies.

## Experimental Section

### *General Procedures*

Our synthetic routes to *anti*-**6** and *syn*-**6** are shown in Scheme<sup>2</sup>. All of the reactions were performed under a dry argon atmosphere. Cyclohexane, 1,4-dioxane, THF, CH<sub>2</sub>Cl<sub>2</sub>, and DMF were guaranteed reagent (GR) grade and stored over molecular sieves. Other reagents were obtained commercially and used without further purification. Reactions were monitored by using TLC. Commercial TLC plates (Merck Co.) were developed and the spots were identified under UV<sup>light</sup> at  $\lambda=254$  and 365<sup>nm</sup>. Column chromatography was performed on

silica gel<sup>60</sup> (0.063--0.200<sup>mm</sup>). All of the synthesized compounds were characterized by using <sup>1</sup>H and <sup>13</sup>C<sup>NMR</sup> spectroscopy and HRMS (FAB); the target compounds were characterized by synchrotron X-ray crystallography.

*Synthesis of 7-tert-Butyl-1-(trimethylsilylethynyl)pyrene (3)*

Trimethylsilylacetylene (1.17<sup>mL</sup>, 8.30<sup>mmol</sup>) and PPh<sub>3</sub> (65.3<sup>mg</sup>, 0.249<sup>mmol</sup>) were added to a stirring solution of 7-tert-butyl-1-bromopyrene (**2**; 1.40<sup>g</sup>, 4.15<sup>mmol</sup>),<sup>[10]</sup> Et<sub>3</sub>N (20<sup>mL</sup>), and THF (20<sup>mL</sup>) and the mixture was stirred at RT under an argon atmosphere. Then, [PdCl<sub>2</sub>(PPh<sub>3</sub>)<sub>2</sub>] (87.2<sup>mg</sup>, 0.125<sup>mmol</sup>), and CuI (23.6<sup>mg</sup>, 0.125<sup>mmol</sup>) were added and the mixture was heated at 80<sup>°C</sup> with stirring for 24<sup>h</sup>. After cooling to RT, the mixture was diluted with CH<sub>2</sub>Cl<sub>2</sub> (200<sup>mL</sup>) and washed successively with saturated aqueous NH<sub>4</sub>Cl solution, water, and brine. The organic layer was dried (MgSO<sub>4</sub>) and the solvents were evaporated. To obtain the pure product, the crude product was purified by column chromatography on silica gel twice (*n*-hexane/CHCl<sub>3</sub>, 9:1) and recrystallized from MeOH to afford the desired compound (**3**) as a light-green solid (1.03<sup>g</sup>, 70% yield).

M.p. 163--164<sup>°C</sup>; <sup>1</sup>H<sup>NMR</sup> (300<sup>MHz</sup>, CDCl<sub>3</sub>): δ=0.39 (s, 9<sup>H</sup>; TMS), 1.59 (s, 9<sup>H</sup>; *t*Bu), 7.98--8.16 (m, 5<sup>H</sup>; pyrene-*H*), 8.23 (s, 1<sup>H</sup>; pyrene-*H*), 8.25 (s, 1<sup>H</sup>; pyrene-*H*), 8.53<sup>ppm</sup> (d, *J*=9.0<sup>Hz</sup>, 1<sup>H</sup>; pyrene-*H*); <sup>13</sup>C<sup>NMR</sup> (100<sup>MHz</sup>, CDCl<sub>3</sub>): δ=31.92, 35.27, 99.99, 104.22, 117.35, 122.51, 122.90, 122.92, 124.17, 124.29, 125.41, 127.09, 128.43, 128.60, 129.63, 130.90, 131.06, 131.23, 132.10, 149.42<sup>ppm</sup>; MS (FAB): *m/z* calcd for C<sub>25</sub>H<sub>26</sub>Si: 354.18 [*M*]<sup>+</sup>; found: 354.17; elemental

analysis calcd (%) for C<sub>25</sub>H<sub>26</sub>Si (354.56): C<sup>84.69</sup>, H<sup>7.39</sup>, Si<sup>7.92</sup>; found: C<sup>84.86</sup>, H<sup>7.21</sup><?><?>no Si, ok?<?><?>.

#### *Synthesis of 7-tert-Butyl-1-ethynylpyrene (4)*

MeOH (20<sup>mL</sup>) and K<sub>2</sub>CO<sub>3</sub> (585<sup>mg</sup>, 4.23<sup>mmol</sup>) were added to a stirring solution of 7-tert-butyl-1-(trimethylsilylethynyl)pyrene (**3**; 1.00<sup>g</sup>, 2.82<sup>mmol</sup>) in THF (20<sup>mL</sup>) and the mixture was stirred at RT for 12<sup>h</sup>. The reaction was quenched by the addition of a large amount of water, extracted with CH<sub>2</sub>Cl<sub>2</sub> (2×50<sup>mL</sup>), washed with water, dried over anhydrous MgSO<sub>4</sub>, and concentrated under vacuum. The residue was recrystallized from MeOH to obtain 7-tert-butyl-1-ethynylpyrene (**4**; 728<sup>mg</sup>, 91% yield) as light-green needles.

M.p. 119--120<sup>°C</sup>; <sup>1</sup>H<sup>NMR</sup> (300<sup>MHz</sup>, CDCl<sub>3</sub>): δ=1.59 (s, 9<sup>H</sup>; tBu), 3.61 (s, 1<sup>H</sup>; C≡C=CH), 8.01 (d, J=8.9<sup>Hz</sup>, 1<sup>H</sup>; pyrene-H), 8.05--8.17 (m, 4<sup>H</sup>; pyrene-H), 8.24 (s, 1<sup>H</sup>; pyrene-H), 8.26 (s, 1<sup>H</sup>; pyrene-H), 8.56<sup>ppm</sup> (d, J=9.2<sup>Hz</sup>, 1<sup>H</sup>; pyrene-H); <sup>13</sup>C<sup>NMR</sup> (100<sup>MHz</sup>, CDCl<sub>3</sub>): δ=31.91, 35.27, 82.41, 82.88, 116.24, 122.45, 122.99, 123.02, 124.17, 124.27, 125.17, 127.04, 128.62, 128.77, 129.82, 130.86, 131.03, 131.44, 132.34, 149.51<sup>ppm</sup>; MS (FAB): m/z calcd for C<sub>22</sub>H<sub>18</sub>: 282.14 [M]<sup><M+></sup>; found: 282.14; elemental analysis calcd (%) for C<sub>22</sub>H<sub>18</sub> (282.38): C<sup>93.57</sup>, H<sup>6.43</sup>; found: C<sup>93.39</sup>, H<sup>6.52</sup>.

#### *Synthesis of Bis(2-tert-butylpyren-6-yl)acetylene (5)*

7-tert-Butyl-1-ethynylpyrene (**4**; 503<sup>mg</sup>, 1.78<sup>mmol</sup>) and PPh<sub>3</sub> (62.2<sup>mg</sup>, 0.237<sup>mmol</sup>) were added to a stirring solution of 7-tert-butyl-1-bromopyrene (**2**; 500<sup>mg</sup>, 1.48<sup>mmol</sup>), Et<sub>3</sub>N (20<sup>mL</sup>), and DMF (20<sup>mL</sup>) and the mixture was stirred at RT under an argon atmosphere. Then, [PdCl<sub>2</sub>(PPh<sub>3</sub>)<sub>2</sub>] (72.8<sup>mg</sup>,

0.104<sup>mmol</sup>) and CuI (31.1<sup>mg</sup>, 0.163<sup>mmol</sup>) were added and the mixture was heated at 100<sup>°C</sup> with stirring for 24<sup>h</sup>. After cooling to RT, the mixture was diluted with CH<sub>2</sub>Cl<sub>2</sub> (200<sup>mL</sup>) and washed successively with saturated aqueous NH<sub>4</sub>Cl solution, water, and brine. The organic layer was dried (MgSO<sub>4</sub>) and the solvents were evaporated. To obtain the pure product, the crude product was purified by column chromatography on silica gel twice (*n*-hexane/CHCl<sub>3</sub>, 3:7) and recrystallized from *n*-hexane/CH<sub>2</sub>Cl<sub>2</sub> (8:2, v/v) to afford the desired compound (**5**) as an orange solid (599<sup>mg</sup>, 75% yield).

M.p. 345--347<sup>°C</sup>; <sup>1</sup>H<sup>NMR</sup> (300<sup>MHz</sup>, CDCl<sub>3</sub>): δ=1.61 (s, 18<sup>H</sup>; *t*Bu), 8.05 (d, *J*=8.8<sup>Hz</sup>, 2<sup>H</sup>; pyrene-*H*), 8.11 (d, *J*=8.8<sup>Hz</sup>, 2<sup>H</sup>; pyrene-*H*), 8.17 (d, *J*=8.0<sup>Hz</sup>, 2<sup>H</sup>; pyrene-*H*), 8.23--8.29 (m, 6<sup>H</sup>; pyrene-*H*), 8.36 (d, *J*=8.0<sup>Hz</sup>, 2<sup>H</sup>; pyrene-*H*), 8.86<sup>ppm</sup> (d, *J*=9.2<sup>Hz</sup>, 2<sup>H</sup>; pyrene-*H*); <sup>13</sup>C<sup>NMR</sup> (100<sup>MHz</sup>, CDCl<sub>3</sub>): δ=31.93, 35.28, 94.46, 117.92, 122.66, 122.95, 124.46, 124.55, 125.59, 127.16, 128.40, 128.70, 129.51, 131.01, 131.17, 131.76, 149.48<sup>ppm</sup>; MS (FAB): *m/z* calcd for C<sub>42</sub>H<sub>34</sub>: 538.27 [*M*]<sup>+</sup>; found: 538.25; elemental analysis calcd (%) for C<sub>22</sub>H<sub>18</sub> (282.38): C<sup>93.64</sup>, H<sup>6.36</sup>; found: C<sup>93.56</sup>, H<sup>6.42</sup>.

*Synthesis of 1,2-Bis(7-tert-butyl-pyren-1-yl)-3,4,5,6-tetraphenylbenzenes (6)*

Compound **5** (100<sup>mg</sup>, 0.279<sup>mmol</sup>) and 2,3,4,5-tetraphenylcyclopenta-2,4-dienone (161<sup>mg</sup>, 0.419<sup>mmol</sup>) were dissolved in Ph<sub>2</sub>O (2.0<sup>mL</sup>) under an argon atmosphere. The mixture was heated at reflux for 24<sup>h</sup> and the solvent was removed under vacuum. The residue was purified by column chromatography on silica gel (CH<sub>2</sub>Cl<sub>2</sub>/*n*-hexane, 4:6) to afford



*anti*-**6** (88.8<sup>^</sup>mg, 53% yield) as a pale-green solid and *syn*-**6** (36.1<sup>^</sup>mg, 22% yield) as a yellow solid.

*anti*-**6**: M.p.<sup>^</sup>>400<sup>^</sup>°C; <sup>1</sup>H<sup>^</sup>NMR (400<sup>^</sup>MHz, CDCl<sub>3</sub>): δ=1.54 (s, 18<sup>^</sup>H; *t*Bu), 6.37--6.48 (m, 4<sup>^</sup>H; Ph-*H*), 6.61 (t, *J*=7.5<sup>^</sup>Hz, 2<sup>^</sup>H; Ph-*H*), 6.78 (d, *J*=7.1<sup>^</sup>Hz, 2<sup>^</sup>H; Ph-*H*), 6.86--7.01 (m, 12<sup>^</sup>H; Ph-*H*), 7.22 (d, *J*=7.9<sup>^</sup>Hz, 2<sup>^</sup>H; pyrene-*H*), 7.46 (d, *J*=9.0<sup>^</sup>Hz, 2<sup>^</sup>H; pyrene-*H*), 7.52 (d, *J*=7.9<sup>^</sup>Hz, 2<sup>^</sup>H; pyrene-*H*), 7.68 (d, *J*=9.0<sup>^</sup>Hz, 2<sup>^</sup>H; pyrene-*H*), 8.00 (d, *J*=9.2<sup>^</sup>Hz, 2<sup>^</sup>H; pyrene-*H*), 8.02 (s, 2<sup>^</sup>H; pyrene-*H*), 8.13 (d, *J*=1.7<sup>^</sup>Hz, 2<sup>^</sup>H; pyrene-*H*), 8.24<sup>^</sup>ppm (d, *J*=9.2<sup>^</sup>Hz, 2<sup>^</sup>H; pyrene-*H*); <sup>13</sup>C<sup>^</sup>NMR (100<sup>^</sup>MHz, CDCl<sub>3</sub>): δ=31.92, 35.11, 121.63, 121.80, 122.69, 123.16, 123.65, 125.14, 125.25, 125.94, 126.33, 126.42, 126.62, 127.28, 128.09, 128.81, 129.12, 130.45, 130.62, 130.87, 131.00, 131.50, 131.71, 135.94, 139.92, 140.05, 140.64, 140.82, 141.66, 148.43<sup>^</sup>ppm; HRMS (FAB MALDI-TOF<?><?>which one<?><?>): *m/z* calcd for C<sub>70</sub>H<sub>54</sub>: 894.4226 [*M*]<sup><M+></sup>; found: 894.4423.

*syn*-**6**: M.p. 214--215<sup>^</sup>°C; <sup>1</sup>H<sup>^</sup>NMR (400<sup>^</sup>MHz, CDCl<sub>3</sub>): δ=1.42 (s, 18<sup>^</sup>H; *t*Bu), 6.36--6.46 (m, 4<sup>^</sup>H; Ph-*H*), 6.57 (t, *J*=7.4<sup>^</sup>Hz, 2<sup>^</sup>H; Ph-*H*), 6.83--6.94 (m, 12<sup>^</sup>H; Ph-*H*), 7.10 (d, *J*=7.5<sup>^</sup>Hz, 2<sup>^</sup>H; Ph-*H*), 7.58 (d, *J*=8.6<sup>^</sup>Hz, 2<sup>^</sup>H; pyrene-*H*), 7.61 (d, *J*=7.5<sup>^</sup>Hz, 2<sup>^</sup>H; pyrene-*H*), 7.66 (d, *J*=8.8<sup>^</sup>Hz, 2<sup>^</sup>H; pyrene-*H*), 7.68 (d, *J*=9.2<sup>^</sup>Hz, 2<sup>^</sup>H; pyrene-*H*), 7.80 (d, *J*=7.9<sup>^</sup>Hz, 2<sup>^</sup>H; pyrene-*H*), 7.89 (s, 4<sup>^</sup>H; pyrene-*H*), 8.23<sup>^</sup>ppm (d, *J*=9.2<sup>^</sup>Hz, 2<sup>^</sup>H; pyrene-*H*); <sup>13</sup>C<sup>^</sup>NMR (100<sup>^</sup>MHz, CDCl<sub>3</sub>): δ=31.81, 34.97, 121.56, 122.61, 122.70, 123.77, 125.10, 125.23, 125.97, 126.26, 126.54, 126.60, 126.63, 126.78, 127.01, 128.88, 129.14, 129.92, 130.48, 130.58, 130.71, 130.81, 131.49, 131.65, 135.69, 140.12, 140.25, 140.71, 140.87, 141.96,

148.09<sup>+</sup>ppm; HRMS (FAB MALDI-TOF<sup>+</sup> which one<sup>+</sup>):  $m/z$  calcd for C<sub>70</sub>H<sub>54</sub>: 894.4426 [M]<sup>+</sup>; found: 894.4418.

## Acknowledgements

This work was performed under the <cgs>Cooperative Research Program</cgs> of the <cgs>Network Joint Research Center for Materials and Devices</cgs> (<cgs>Institute for Materials Chemistry and Engineering, Kyushu University</cgs>). We thank the <cgs>National Science Foundation of China</cgs> (<cn>21602014</cn>), the <cgs>Fund Program for the Scientific Activities of Selected Returned Overseas Professionals of Beijing</cgs>, the <cgs>OTEC</cgs> at <cgs>Saga University</cgs>, and the <cgs>International Cooperation Projects of Guizhou Province</cgs> (<cn>20137002</cn>) for financial support and the <cgs>EPSRC</cgs> for an overseas travel grant to C.R. The Advanced Light Source is supported by the <cgs>Director, Office of Science, Office of Basic Energy Sciences</cgs>, of the <cgs>U.S. Department of Energy</cgs> (<cn>DE-AC02-05CH11231</cn>).

## Conflict of interest

The authors declare no conflict of interest.

<lit1><lit\_a><jnl>K.-R. Wee, W.-S. Han, D.<sup>+</sup>W. Cho, S. Kwon, C. Pac, S.<sup>+</sup>O. Kang, *Angew. Chem. Int. Ed.* **2012**, 51, 2677--2680; *Angew. Chem.* **2012**, 124, 2731--2734</jnl>;  
<lit\_b><jnl>K.-R. Wee, Y.-J. Cho, J.<sup>+</sup>K. Song, S.<sup>+</sup>O. Kang, *Angew. Chem. Int. Ed.* **2013**, 52, 9682--9685; *Angew. Chem.* **2013**, 125, 9864--9867</jnl>.

- <lit2><lit\_a><jnl>P.<sup>^</sup>I. Shih, C.<sup>^</sup>Y. Chuang, C.<sup>^</sup>H. Chien, E.<sup>^</sup>W.<sup>^</sup>G. Diau, C.<sup>^</sup>F. Shu, *Adv. Funct. Mater.* **2007**, 17, 3141--3146</jnl>; <lit\_b><jnl>Z. Zhao, P. Lu, J.<sup>^</sup>W.<sup>^</sup>Y. Lam, Z. Zhang, C.<sup>^</sup>Y.<sup>^</sup>K. Chan, H.<sup>^</sup>H.<sup>^</sup>Y. Sung, I.<sup>^</sup>D. Williams, Y. Ma, B.<sup>^</sup>Z. Tang, *Chem. Sci.* **2011**, 2, 672--675</jnl>; <lit\_c><jnl>Z. Zhao, S. Chen, C.<sup>^</sup>Y.<sup>^</sup>K. Chan, J.<sup>^</sup>W.<sup>^</sup>Y. Lam, C.<sup>^</sup>K.<sup>^</sup>W. Jim, P. Lu, Z. Chang, H.<sup>^</sup>S. Kwok, H. Qiu, B.<sup>^</sup>Z. Tang, *Chem. Asian J.* **2012**, 7, 484--488</jnl>; <lit\_d><jnl>Z. Zhao, S. Chen, J.<sup>^</sup>W.<sup>^</sup>Y. Lam, P. Lu, Y. Zhong, K.<sup>^</sup>S. Wong, H.<sup>^</sup>S. Kwok, B.<sup>^</sup>Z. Tang, *Chem. Commun.* **2010**, 46, 2221--2223</jnl>.
- <lit3><lit\_a><jnl>M. Gingras, *Chem. Soc. Rev.* **2013**, 42, 968--1006</jnl>; <lit\_b><jnl>T. Fujikawa, Y. Segawa, K. Itami, *J. Am. Chem. Soc.* **2015**, 137, 7763--7768</jnl>; <lit\_c><jnl>T. Fujikawa, Y. Segawa, K. Itami, *J. Am. Chem. Soc.* **2016**, 138, 3587--3595</jnl>.
- <lit4><lit\_a><jnl>L. Sánchez, R. Otero, J.<sup>^</sup>M. Gallego, R. Miranda, N. Martín, *Chem. Rev.* **2009**, 109, 2081--2091</jnl>; <lit\_b><jnl>P. Moreno-García, A.<sup>^</sup>L. Rosa, V. Kolivoška, D. Bermejo, W.<sup>^</sup>J. Hong, K. Yoshida, M. Baghernejad, S. Filippone, P. Broekmann, T. Wandlowski, N. Martín, *J. Am. Chem. Soc.* **2015**, 137, 2318--2327</jnl>.
- <lit5><lit\_a><jnl>R.<sup>^</sup>R. Hu, J.<sup>^</sup>W.<sup>^</sup>Y. Lam, Y. Liu, X. Zhang, B.<sup>^</sup>Z. Tang, *Chem. Eur. J.* **2013**, 19, 5617--5624</jnl>; <lit\_b><jnl>V. Vij, V. Bhalla, M. Kumar, *Chem. Rev.* **2016**, 116, 9565--9627</jnl>; <lit\_c><jnl>D. Lungerich, D. Reger, H. Hölzel, R. Riedel, M.<sup>^</sup>J.<sup>^</sup>C. Martin, F. Hampel, N. Jux, *Angew. Chem. Int. Ed.* **2016**, 55, 5602--5605; *Angew. Chem.* **2016**, 128, 5692--5696</jnl>.

- <lit6><lit\_a><jnl>T. M. Figueira-Duarte, K. Müllen, *Chem. Rev.* **2011**, *111*, 7260--7314</jnl>; <lit\_b><jnl>X. Feng, J. Y. Hu, C. Redshaw, T. Yamato, *Chem. Eur. J.* **2016**, *22*, 11898--11916</jnl>.
- <lit7><jnl>D. A. Safin, M. G. Babashkina, M. P. Mitoraj, P. Kubisiak, K. Robeyns, M. Bolte, Y. Garcia, *Inorg. Chem. Front.* **2016**, *3*, 1419--1431</jnl>.
- <lit8><lit\_a><jnl>T. Förster, *Angew. Chem. Int. Ed. Engl.* **1969**, *8*, 333--343; *Angew. Chem.* **1969**, *81*, 364--374</jnl>; <lit\_b><jnl>A. Ueno, I. Suzuki, T. Osa, *J. Am. Chem. Soc.* **1989**, *111*, 6391--6397</jnl>; <lit\_c><jnl>B. Zhao, N. Li, X. Wang, Z. Chang, X. H. Bu, *ACS Appl. Mater. Interfaces* **2017**, *9*, 2662--2668</jnl>; <lit\_d><jnl>C. Z. Wang, H. Ichiiyanagi, K. Sakaguchi, X. Feng, M. R. J. Elsegood, C. Redshaw, T. Yamato, *J. Org. Chem.* **2017**, *82*, 7176--7182</jnl>.
- <lit9><jnl>H. J. Ju, K. Wang, J. Zhang, H. Geng, Z. T. Liu, G. X. Zhang, Y. S. Zhao, D. Q. Zhang, *Chem. Mater.* **2017**, *29*, 3580--3588</jnl>.
- <lit10><jnl>X. Feng, J. Y. Hu, H. Tomiyasu, Z. Tao, C. Redshaw, M. R. J. Elsegood, L. Horsburgh, S. J. Teat, X. F. Wei, T. Yamato, *RSC Adv.* **2015**, *5*, 8835--8848</jnl>.
- <lit11><jnl>A. G. Crawford, A. D. Dwyer, Z. Q. Liu, A. Steffen, A. Beeby, L.-O. Palsson, D. J. Tozer, T. B. Marder, *J. Am. Chem. Soc.* **2011**, *133*, 13349--13362</jnl>.
- <lit12><jnl>L. J. Sun, W. G. Zhu, W. Wang, F. X. Yang, C. C. Zhang, S. F. Wang, X. T. Zhang, R. J. Li, H. L.

- Dong, W.<sup>^</sup>P. Hu, *Angew. Chem. Int. Ed.* **2017**, 56, 7831--7835; *Angew. Chem.* **2017**, 129, 7939--7943</jnl>.
- <lit13><lit\_a><jnl>Z.<sup>^</sup>K. Wang, J.<sup>^</sup>Y. Nie, W. Qin, Q.<sup>^</sup>L. Hu, B.<sup>^</sup>Z. Tang, *Nat. Commun.* **2016**, 7, 12033</jnl>;
- <lit\_b><jnl>G. Singh, S.<sup>^</sup>I. Reja, V. Bhalla, D. Kaur, P. Kaur, S. Arora, M. Kumar, *Sens. Actuators B* **2017**, 249, 311--320</jnl>; <lit\_c><jnl>J. Mei, N.<sup>^</sup>L.<sup>^</sup>C. Leung, R.<sup>^</sup>T.<sup>^</sup>K. Kwok, J.<sup>^</sup>W.<sup>^</sup>Y. Lam, B.<sup>^</sup>Z. Tang, *Chem. Rev.* **2015**, 115, 11718--11940</jnl>.
- <lit14><lit\_a><jnl>H. Li, Z. Chi, X. Zhang, B. Xu, S. Liu, Y. Zhang, J. Xu, *Chem. Commun.* **2011**, 47, 11273--11275</jnl>;
- <lit\_b><jnl>T. Jadhav, B. Dhokale, Y. Patil, S.<sup>^</sup>M. Mobin, R. Misra, *J. Phys. Chem. C* **2016**, 120, 24030--24040</jnl>.

Manuscript received: October 11, 2017

Revised manuscript received: November 27, 2017

Accepted manuscript online: <?><?>

Version of record online: <?><?>

Scheme<sup>^</sup>1 Illustration of the typical structures that give rise to emissions from the pyrene system.

Scheme<sup>^</sup>2 Our synthetic route to *anti*-**6** and *syn*-**6**.

TMS=trimethylsilyl, BTMABr<sub>3</sub>=benzyltrimethylammonium tribromide.<?><?>definition ok<?><?>

Figure<sup>^</sup>1 Two orthogonal views of the crystal structures of *anti*-**6** (a) and *syn*-**6** (b); hydrogen atoms are omitted for clarity.

Figure<sup>^</sup>2 Partial <sup>1</sup>H<sup>^</sup>NMR spectra (400<sup>^</sup>MHz, 25<sup>^</sup>°C, CDCl<sub>3</sub>) of *anti*-**6** (top) and *syn*-**6** (bottom).

Figure<sup>3</sup> UV/Vis absorption spectra in THF solution, and fluorescence spectra in THF solution and in the solid state of *anti*-**6** and *syn*-**6**.

Figure<sup>4</sup> Packing structures of *anti*-**6** (a) and *syn*-**6** (b), with principal intermolecular packing interactions. Most hydrogen atoms are omitted for clarity; distances are in [Å].

Figure<sup>5</sup> a) PL spectra of *anti*-**6** in THF/water mixtures ( $5 \times 10^{-7}$  M); b) plot of  $I/I_0$  versus  $f_w$  for *anti*-**6** in THF/water mixtures.  $f_w$ =water fraction.

Table<sup>1</sup> Photophysical properties of HAB derivatives *anti*-**6** and *syn*-**6**.

Py-based HAB	Transition	$\lambda_{\text{Abs}}$ [nm] [a]	$\log \epsilon$ [ $\text{M}^{-1}\text{cm}^{-1}$ ]	$\lambda_{\text{PL}}$ [nm] [a]	$\lambda_{\text{PL}}$ [nm] [b]
<i>anti</i> - <b>6</b>	$S_0 \rightarrow S_1$	403	2.87	394 (dp), 447	463
	$S_0 \rightarrow S_2$	353	4.72		482
	$S_0 \rightarrow S_3$	283	4.67		
<i>syn</i> - <b>6</b>	$S_0 \rightarrow S_1$	404	3.62	412	420
	$S_0 \rightarrow S_2$	334	4.68		484
	$S_0 \rightarrow S_3$	272	4.76		

[a] Measured in THF at RT; [b] measured as a powder;

[c] the fraction of water in a water/THF mixed solvent system is shown in parentheses; [d] DFT calculations were performed

at the B3LYP/6-31G\* level of theory; [e] determined from the oxidation potential in THF by using cyclic voltammetry;

[f]  $E_{\text{LUMO}} - E_{\text{HOMO}}$ ; [g] estimated from the absorption edge of the UV/Vis spectrum.